ACS OMEGA

http://pubs.acs.org/journal/acsodf

Article

Applications of Polyaniline-Based Molybdenum Disulfide Nanoparticles against Brain-Eating Amoebae

Sumayah Abdelnasir, Mohammad Ridwane Mungroo, Jactty Chew, Ruqaiyyah Siddiqui, Naveed Ahmed Khan, Irfan Ahmad, Syed Shahabuddin,* and Ayaz Anwar*

Cite This: *ACS Omega* 2023, 8, 8237–8247

Read Online

ACCESS | Metrics & More | Article Recommendations

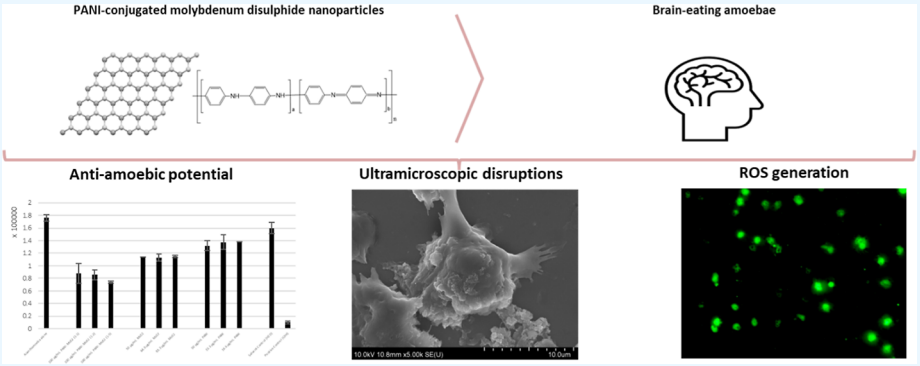

ABSTRACT: Primary amoebic meningoencephalitis and granulomatous amoebic encephalitis are distressing infections of the central nervous system caused by brain-eating amoebae, namely, *Naegleria fowleri* and *Acanthamoeba* spp., respectively, and present mortality rates of over 90%. No single drug has been approved for use against these infections, and current therapy is met with an array of obstacles including high toxicity and limited specificity. Thus, the development of alternative effective chemotherapeutic agents for the management of infections due to brain-eating amoebae is a crucial requirement to avert future mortalities. In this paper, we synthesized a conducting polymer-based nanocomposite entailing polyaniline (PANI) and molybdenum disulfide (MoS_2) and explored its anti-trophozoite and anti-cyst potentials against *Acanthamoeba castellanii* and *Naegleria fowleri*. The intracellular generation of reactive oxygen species (ROS) and ultrastructural appearances of amoeba were also evaluated with treatment. Throughout, treatment with the 1:2 and 1:5 ratios of PANI/MoS_2 at 100 μg/mL demonstrated significant anti-amoebic effects toward *A. castellanii* as well as *N. fowleri*, appraised to be ROS mediated and effectuate physical alterations to amoeba morphology. Further, cytocompatibility toward human keratinocyte skin cells (HaCaT) and primary human corneal epithelial cells (pHCEC) was noted. For the first time, polymer-based nanocomposites such as PANI/MoS_2 are reported in this study as appealing options in the drug discovery for brain-eating amoebae infections.

INTRODUCTION

Acanthamoeba spp. and *Naegleria fowleri* are among the four genera of free-living amoebae that are known to cause infections in humans.[1] These amoebae are aerobic eukaryotic protozoa and pose grave clinical problems with new cases being reported worldwide. Ubiquitously distributed in natural environments as well as artificial water systems, *A. castellanii* and *N. fowleri* are the causative agents of fatal central nervous system (CNS) infections namely granulomatous amoebic encephalitis (GAE) and primary amoebic meningoencephalitis (PAM), respectively, and thus are duly termed "brain-eating amoebae".[2] Although rare, these infections are accompanied with devastating clinical manifestations and mortality rates over 95%, yet any well-established treatment is lacking.[3]

N. fowleri is believed to employ the nasal route in invading the host followed by locomotion through the olfactory nerves up to the olfactory bulbs, activating significant innate immune response and consequentially causing PAM.[4] This infection manifests as substantial nerve damage and hemorrhaging necrosis of meninges and other CNS tissue, almost always resulting in death.[5] Similarly, GAE is a fatal condition that ensues *A. castellanii* access to the host through the respiratory tract, eyes, or skin lesions.[6] Invasion of the blood stream and the hematogenous spread of amoeba expose it to the brain.

Received: September 19, 2022
Accepted: December 16, 2022
Published: February 24, 2023

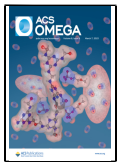

Here, the formation of granulomas, abscesses, and necrosis of CNS tissue including the brainstem, cerebellum, and cerebral hemisphere are responsible for death in over 95% of cases.[7] In addition to GAE, *A. castellanii* is also the causal agent of a blinding corneal infection—*Acanthamoeba*keratitis (AK) associated mainly with contact lens wearers.[8]

No specific treatment for these cerebral infections due to brain-eating amoebae exists. Current therapy includes the combination of several drugs with various modes of action.[2] These include different groupings of azoles such as fluconazole and voriconazole, amphotericin B, rifampin, and polyhexamethylene biguanides for the treatment of GAE.[9] Comparably, PAM is typically treated with a cocktail constituting amphotericin B, miltefosine, miconazole, azithromycin, and dexamethasone, among others.[10] However, adverse effects including nephrotoxicity have been reported as a result of treatment of PAM.[11] Further, these current treatment options for brain-eating amoeba infections are more often than not limited by their high host cell cytotoxicity and lack of specificity for the amoeba.[12] This is on top of their inability to permeate the blood−brain barrier (BBB) sufficiently enough to reach therapeutic doses.[13] In addition, a major hindrance to effective treatment is the recurrence of these CNS infections due to resistant double-walled cyst stages of the parasites that persist in the host despite therapy.[14] Overall, there is a critical, unmet necessity for the development of effective, BBB-permeable, and alternative therapy for the control of cerebral infections due to brain-eating amoebae.

In light of alternative therapy, non-conventional antimicrobials such as nanomaterials have garnered significant scientific interest for their use against a variety of microorganisms.[15] This is primarily due to the surface functionalization properties that nanoparticles offer in addition to multiple reported modes of microbial inhibition, making resistance development difficult.[16] The surface of nanoparticles facilitates modification with therapeutic moieties as well as guiding molecules such as peptides and antibodies. In addition, DNA interaction, reactive oxygen species (ROS) provocation, and mechanical membrane damage are a few mechanisms studied to be employed by nanomaterials in inhibiting microbes.[17] Owing to their unique properties and wide applicability, ultrathin two-dimensional transition metal dichalcogenides (TMDCs) have attained phenomenal research interest.[18] Molybdenum disulfide (MoS_2) is a highly typical member of the TMDC class of compounds that have the chemical formula MX_2, wherein M is representative of a transition metal and X represents a chalcogen element.[19] Typically, TMDCs exist in X-M-X layers held together by weak van der Waals forces with strong covalent bonds between atoms within each layer. MoS_2-based nanomaterials show considerable promise for their use in a variety of fields including biomedical applications.[20] High antimicrobial activity of MoS_2 nanomaterials has been repeatedly reported toward resistant Gram-positive and Gram-negative bacteria through the generation of ROS and free radicals as well as metabolic inactivation and membrane integrity depletion.[21] In addition, the in vitro and in vivo host compatibility of TMDC nanomaterials including MoS_2 has been evaluated to be superior than their carbon analogues.[22] Low cytotoxicity and genotoxicity were also studied to be exhibited by MoS_2 as well as its nanomaterials, in particular.[23] Still, the effects of TMDC-based nanomaterials are yet to be explored apropos of anti-parasitic behavior.

In spite of its positive attributes, the limited colloidal aqueous stability of MoS_2 is a major limitation associated with its use.[20b] In addressing these limitations, the facile surface functionalization[24] of MoS_2 is exploited to enhance its stability with the incorporation of supporting materials including polymers.[25] Conducting polymers such as polyaniline (PANI) are well acknowledged in the scientific community for their processability, stability, easy synthesis, low cost, as well as electrical and optical properties.[26] In addition to improving the stability of MoS_2, the integration of a nanoscale component within a polymer matrix has been appreciated to generate a composite with ameliorated properties relative to either individual material.[27] In the hybrid, nanoparticle aggregation, which significantly affects its practical application, is inhibited, and the limited solubility of PANI would also be diminished, rendering an overall superior material.[28] Further, the in vitro and in vivo biocompatibility of PANI have been extensively explored.[29] We have previously shown that PANI-based nanocomposites incorporated with boron nitride and tungsten disulfide exhibit potent amoebicidal and cysticidal effects against brain-eating amoebae.[30]

For these qualities, in this study, we have synthesized a nanocomposite based on PANI and MoS_2, PANI/MoS_2, and explored its anti-amoebic aptitude toward *N. fowleri* and *A. castellanii*.

RESULTS AND DISCUSSION

Clinically, effective treatment of CNS infections due to *A. castellanii* and *N. fowleri* is faced with an array of obstacles including but not limited to the toxicity due to high dosages required for administered drugs to permeate the BBB at sufficient amounts.[1] Other hindrances include the recurrence of infection due to persevering cysts and adverse effects as a result of toxicity.[2] These impediments have largely contributed to the increasing mortality rates of CNS infections due to brain-eating amoebae and mandate alternative effective treatment.

For these reasons, we synthesized a nanocomposite based on PANI and MoS_2 and explored its effects toward brain-eating amoebae. Such nanocomposites constituting polymers have been noted to retain enhanced features relative to the individual materials with regard to stability and the inhibition of nanoparticle aggregation. Further, it has been acknowledged in literature that MoS_2-based nanoplatforms exhibit antimicrobial properties.[21,31] Likewise, PANI-based nanocomposites have also been commended as promising antimicrobials.[32] Based on these motives, for the first time, we explored the effects of PANI:MoS_2 on the viability of the trophozoite and cyst stages of *N. fowleri* as well as *A. castellanii*.

Morphology of PANI, MoS_2, and PANI-MoS_2 Nanocomposites. FE-SEM and TEM techniques were used to thoroughly study the morphology of PANI, MoS_2 nanosheets, and MoS_2-doped PANI nanocomposites. The MoS_2 surface morphology is shown in Figures 1a,b. From Figure 1a, it is seen that the morphology of MoS_2 in the nano-range depicts stacked sheets, and Figure 1b shows highly stacked 2D sheets of MoS_2 nanosheets. As shown in Figure 1c, PANI displays a tubular shape, and the tubes' measurement ensures that nanotubes have been formed. Figure 1d shows the micrograph of P−MoS_2 nanocomposite. The image shows the granular polymeric network after the transformation from PANI nanotubes. There is no significant change in the morphology by the addition of MoS_2 nanosheets, but the result clearly

https://doi.org/10.1021/acsomega.2c06050
ACS Omega 2023, 8, 8237−8247

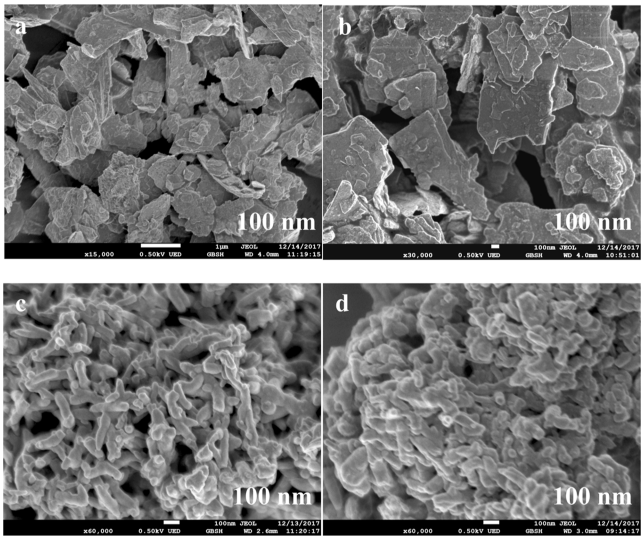

Figure 1. FE-SEM micrographs of (a,b) MoS_2 nanosheets (c) PANI nanotubes, and (d) PANI/MoS_2 (1:5) nanocomposite.

shows that the surface has changed to become considerably more granular. Moreover, because the concentration of PANI is much higher than that of MoS_2, it is difficult to see MoS_2 nanosheets in the nanocomposite.

TEM analyses of MoS_2 nanosheets and PANI-MoS_2 nanocomposites were carried out to further support their formation. The TEM image of MoS_2 is shown in Figure 2a,

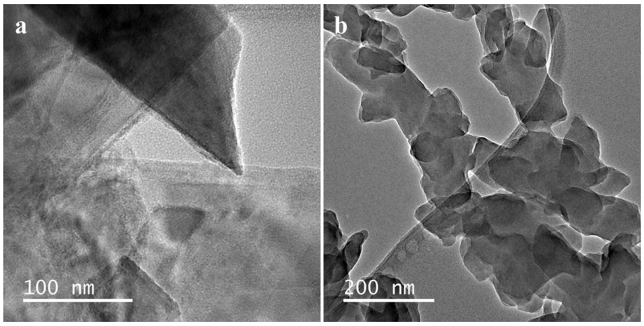

Figure 2. TEM micrographs of (a) MoS_2 nanosheets (b) PANI/MoS_2 (1:5) nanocomposite.

which depicts the disc-shaped morphology, and molecular fringes demonstrate the pure crystalline phase of MoS_2. Additionally, the MoS_2 HRTEM image displayed a layer with the interlayer distance of 2.5 Å, which is the typical N−N interlayer distance of MoS_2 lattice. As can be seen in Figure 2b, the formation of P−MoS_2 nanocomposite is confirmed by the disc-like nanospheres that are embedded inside the PANI's tubular structure. As a result, the formation of PANI nanotubes and MoS_2-doped PANI composites is clear from FE-SEM and TEM images.

PANI/MoS_2 Revealed Minimal Cytotoxicity towards Skin and Corneal Cells. Among factors considered in drug development, the toxicity and biocompatibility of candidates toward host cells take leading priority. Thus, we employed lactate dehydrogenase (LDH) reagents to assess the cytotoxicity of PANI/MoS_2 toward human keratinocyte skin cells (HaCaT). Its toxicity was also explored toward primary human corneal epithelial cells (pHCEC) because of the relevance of this cell line to *Acanthamoeba* keratitis due to *A. castellanii*. As described, 100 μg/mL of PANI/MoS_2 at varying ratios (1:1, 1:2, and 1:5) was added to 96-well plates containing monolayers of human cells in RPMI-1640. The plates were incubated for 24 h before LDH release was quantified spectrophotometrically as an indicator of cell death. The LDH reagent kit (Roche) was used to quantify the levels of LDH in the supernatant of treated human cells as a measure of spectrophotometric absorbance. This was valued as a percentage between maximal (positive control) and minimum (negative control) cytotoxicity. Overall, the nanocomposite (PANI/MoS_2) and components alone (PANI and MoS_2) displayed minimal toxic effects toward HaCaT cells (Figure 3a). At the 1:1 and 1:2 formulations of PANI/MoS_2, no cytotoxicity was measured. However, this was increased with a higher proportion of MoS_2 in PANI/MoS_2 (1:5) which elicited 15% HaCaT cell death. At the higher concentration of MoS_2 alone (83.3 μg/mL), 9% cytotoxicity toward the skin cells was observed. Likewise, no cytotoxicity toward HaCaT cells was noted after incubation with PANI alone, except at 50 μg/mL of the polymer (9% cell death).

Similar cytotoxicity was observed to be spawned by the nanocomposite toward pHCEC. PANI/MoS_2 (1:1) at 100 μg/mL generated 3.2% cytotoxicity toward pHCEC. Increasing the MoS_2 component by two folds, in the 1:2 ratio of the nanocomposite, did not markedly affect toxicity, maintaining pHCEC cell death at 4.5%. However, PANI/MoS_2 at a ratio of 1:5 caused an increased cytotoxicity toward corneal cells (26%) relative to its 1:1 and 1:2 variants. Lastly, the component controls (PANI alone and MoS_2 alone) also demonstrated minimal toxic effects toward corneal cells. For instance, up to 500 μg/mL of the MoS_2 alone and up to 100 μg/mL of PANI alone only caused 2.9 and 5% pHCEC death, respectively (Figure 3b).

In literature, TMDCs including MoS_2 have been analyzed to surpass their graphene analogues in numerous aspects including biocompatibility and in vitro as well as in vivo cytocompatibility.[22] The minimal cytotoxicity of the nanomaterials of MoS_2 including polymer-based structures has been described repeatedly. Up to 200 μg/mL of MoS_2 nanoplatforms were reported to exhibit no toxicity toward human renal epithelial cells 293T, HeLa cells, as well as mouse macrophage RAW 264.7.[33] Further, Mukheem et al.[34] also deem biopolymer-based MoS_2 nanosheets as safe to use in biomedical applications owing to their cytocompatibility with HaCaT cells. In vivo studies in BALB/c mice demonstrated the complete excremental clearance of MoS_2-based nanostructures and negligible toxicity.[35] On another note, as aforementioned, PANI and PANI-based nanomaterials have been extensively explored to retain positive compatibility in vitro as well as in vivo. Overall, similar to earlier reports, PANI/MoS_2 nanocomposite can be reasonably recognized as safe toward human cells in vitro.

PANI/MoS_2 Displayed Significant Trophocidal Effects against *A. castellanii*. The in vitro anti-amoebic capacity of PANI/MoS_2 is an imperative factor, essential for gauging its therapeutic properties. This capability was evaluated in amoebicidal assays using 100 μg/mL PANI/MoS_2 at three ratios (1:1, 1:2, and 1:5) (Figure 4a). The anti-trophozoite potential of PANI alone (50, 33.3, and 16.6 μg/mL) and MoS_2 alone (50, 66.6, and 83.3 μg/mL) was also explored. IC_{50} was achieved by 100 μg/mL of PANI/MoS_2 in all the three ratios tested. PANI/MoS_2 (1:1) decreased viable *A. castellanii*

https://doi.org/10.1021/acsomega.2c06050
ACS Omega 2023, 8, 8237−8247

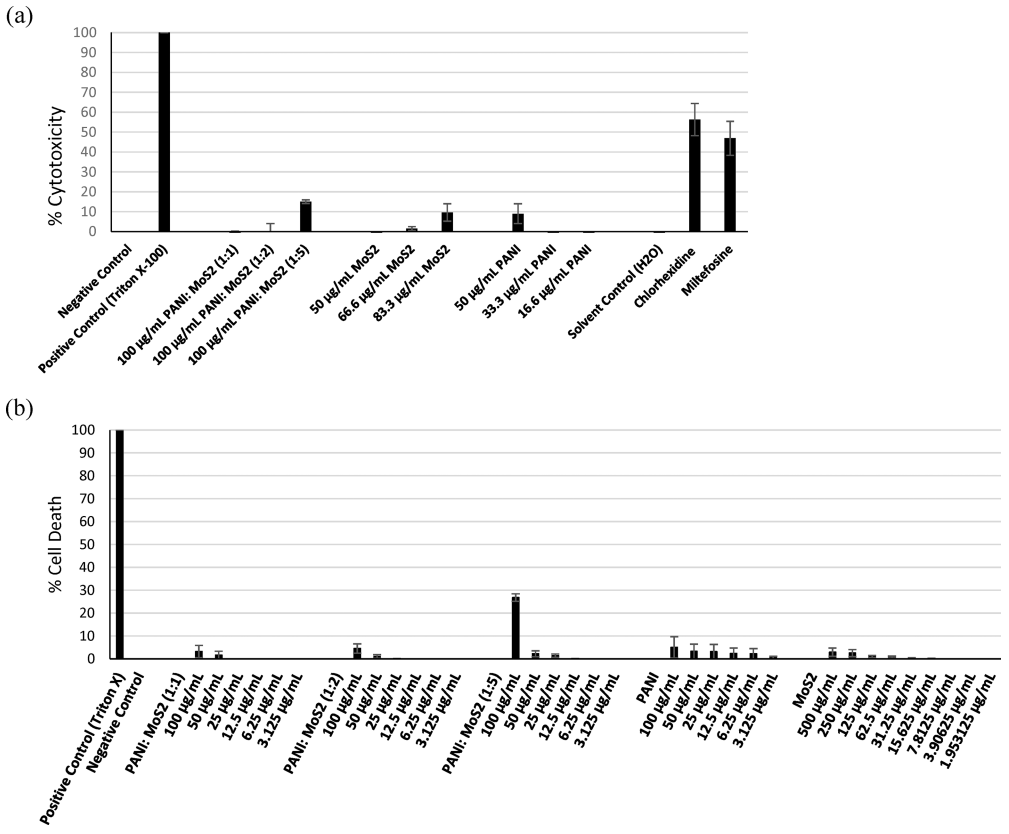

Figure 3. Host cell cytotoxic effects of up to 100 μg/mL PANI/MoS_2 (1:1, 1:2, and 1:5) and component controls at equivalent concentrations toward (a) human keratinocyte skin cells (HaCaT) and (b) pHCEC. In brief, PANI/MoS_2 and controls were incubated with monolayers of HaCaT cells and pHCEC at 37 °C in a 95% humidified, 5% CO_2 incubator for 24 h. The results show that PANI/MoS_2 elicits limited host cell damage. The data displayed is the mean ± standard error of multiple experiments performed in duplicates.

trophozoite numbers by 50%, from 1.76×10^5 in the negative control to 8.8×10^4 cells. Similarly, the 1:2 and 1:5 formulations of the nanocomposite instigated 51 and 58% inhibition of viability, respectively. These ratios exhibited the statistically significant reduction in trophozoite numbers compared to the negative control (*$P < 0.05$). The 58% inhibition caused by 100 μg/mL of PANI/MoS_2 (1:5) was analyzed to be significant also relative to the component controls (PANI alone and MoS_2 alone) at respective concentrations (##$P < 0.005$, in comparison to component controls). This is notwithstanding the noteworthy viability inhibition (35%) produced as a result of *A. castellanii* trophozoite treatment with 83.3 μg/mL of MoS_2 alone. Treatment with PANI alone did not demonstrate significant effects on the viability of *A. castellanii* trophozoites—25% inhibition with 50 μg/mL of the polymer (Figure 4a). From these values, it is logical to infer that the incorporation of either component into a nanocomposite enhanced their individual in vitro anti-amoebic abilities.

PANI/MoS_2 (1:5) at 100 μg/mL Reduced the Number of *A. castellanii* Cysts to 60%. The anti-cyst capacity of potential therapy for amoeba infections is a crucial factor to consider as these are the resistant stages of the amoeba that are attributable to recurring infections and, in turn, ineffective treatment. Hence, we conducted cysticidal assays to verify the capacity of PANI/MoS_2 to inhibit cysts. 100 μg/mL of the nanocomposite at three formulations (1:1, 1:2, and 1:5) was used to treat mature *A. castellanii* cysts for 24 h as described (Figure 4b). All three ratios of 100 μg/mL of PANI/MoS_2 yielded statistically significant inhibitions of cyst viability relative to the negative control (1.065×10^5 viable cysts) (*$P < 0.05$). Relative to the negative control, numbers of viable cysts were reduced by 44% to 6.0×10^4 due to 100 μg/mL PANI/MoS_2 (1:1). The 1:2 and 1:5 ratios of the nanomaterial generated 54 and 60% inhibition of *A. castellanii* cyst viability, respectively—significant compared to the negative control as well as component controls (MoS_2 alone and PANI alone) at appropriate concentrations (#$P < 0.05$, in comparison to component controls). In contrast, PANI alone and MoS_2 alone did not return notable effects toward *A. castellanii* cysts, maintaining viability at about 70 and 67%, respectively, at their maximum tested concentrations (Figure 4b).

Overall, consistent with anti-trophozoite experiments, the 1:5 ratio transcended the other ratios apropos of the in vitro anti-*A. castellanii* capacity. Further, once again, the nanocomposite (1:2 and 1:5) demonstrated significantly enhanced cysticidal activities relative to either component alone (Figure 4b).

PANI/MoS_2 Caused Death of *N. fowleri* Trophozoites. The anti-amoebic potential of PANI/MoS_2 was also explored toward the amoeba of a different genera—*N. fowleri*. 100 μg/mL PANI/MoS_2 at three ratios (1:1, 1:2, and 1:5) was incubated with *N. fowleri* trophozoites for 24 h as described previously (Figure 5a). All the ratios tested demonstrated statistically significant depletion of trophozoite viability compared to the negative control (*$P < 0.05$ and #$P < 0.05$, in comparison to PANI and MoS_2 alone). For instance, the 1:1 and 1:5 ratios of the nanocomposite at 100 μg/mL spawned 40

https://doi.org/10.1021/acsomega.2c06050
ACS Omega 2023, 8, 8237−8247

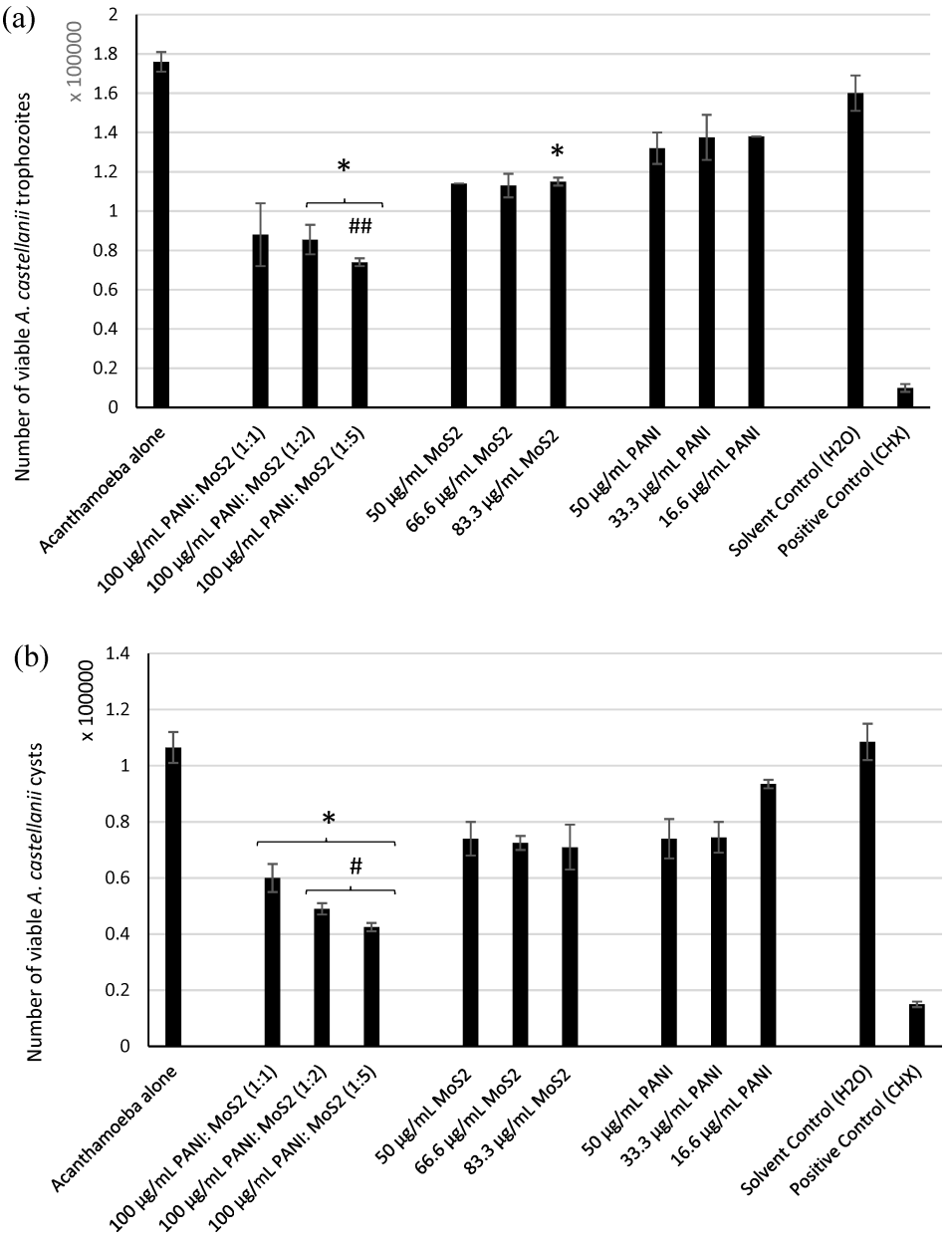

Figure 4. Anti-amoebic effects of PANI/MoS_2 (1:1, 1:2, and 1:5) at 100 μg/mL as well as PANI alone and MoS_2 alone, at corresponding concentrations on *A. castellanii* (a) trophozoites and (b) cysts. In short, PANI/MoS_2 and controls were used to treat 2.5 × 10^5 *A. castellanii* trophozoites and cysts incubated at 30 °C for 24 h in amoebicidal and cysticidal assays, respectively. After the incubation time, live cells were distinguished (unstained) and enumerated in Trypan Blue exclusion assays. The results show significant amoebicidal (*P < 0.05, using two sampled t-test, two-tailed distribution, ##P < 0.005, in comparison to component controls) and cysticidal activities (*P < 0.05 and #P < 0.05).

and 49% *N. fowleri* trophozoite death, respectively, in comparison to the negative control. Interestingly, the 1:2 formulation generated the IC_{50} of PANI/MoS_2 (100 μg/mL) against *N. fowleri* trophozoites, eliciting 53% viability inhibition. When juxtaposed with the component controls, it was noted that MoS_2 alone (83.3 μg/mL) insignificantly inhibited trophozoite viability by 30%. Likewise, 50 μg/mL of PANI alone elicited 23% *N. fowleri* trophozoite death (Figure 5a). Considering these values, it can be deduced that the amalgamation of PANI and MoS_2 is attributable for the comparatively augmented anti-trophozoite potential of PANI/MoS_2.

PANI/MoS_2 Exhibited Anti-Cyst Effects against *N. fowleri*. Owing to the resistance of double-walled *N. fowleri* cysts, infections due to this protozoan are well-known to recur. Hence, cysticidal activity is a chief prerequisite of the potential drugs for these infections. The anti-*N. fowleri* cyst effects of PANI/MoS_2 were examined in cysticidal assays using 100 μg/mL of the composite as aforementioned (Figure 5b). Coherent with anti-trophozoite assays, the 1:2 ratio of PANI/MoS_2 maintained superiority over other formulations in inhibiting *N. fowleri* cysts, generating 40% cell death. This cyst viability exhaustion is statistically significant relative to the negative control as well as the components (PANI and MoS_2) alone (*P < 0.05 and #P < 0.05, in comparison to component controls). In contrast, the 1:1 and 1:5 ratios of PANI/MoS_2 did not prominently inhibit *N. fowleri* cysts producing 25 and 30% cell death, respectively. Overall, it can be understood that

https://doi.org/10.1021/acsomega.2c06050
ACS Omega 2023, 8, 8237−8247

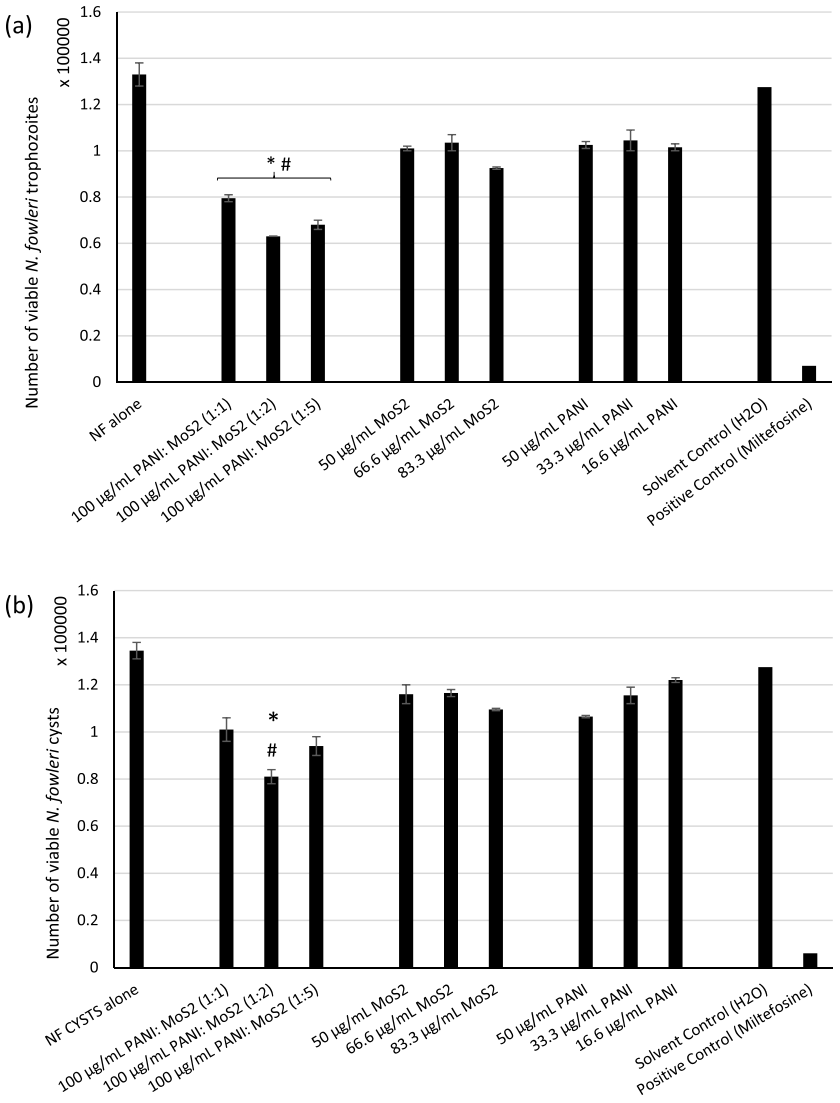

Figure 5. Anti-amoebic effects of 100 μg/mL of PANI/MoS_2 (1:1, 1:2, and 1:5) and the respective concentrations of controls on *N. fowleri* (a) trophozoites and (b) cysts. Briefly, 2.5×10^5 *N. fowleri* trophozoites and cysts were treated with PANI/MoS_2 and controls (PANI alone and MoS_2 alone) for 24 h at 30 °C in (a) anti-trophozoite and (b) anti-cyst assays, respectively. Subsequently, live cells were enumerated after the staining of non-viable cells in Trypan Blue exclusion assays. The results show significant amoebicidal and cysticidal activities (*$P < 0.05$, using two sampled *t*-test, two-tailed distribution) (#$P < 0.05$, in comparison to compound controls).

the anti-cyst capacity of 100 μg/mL PANI/MoS_2 (1:2) was not due to either individual component—both of which maintained more than 80% cyst viability—but rather their assimilation into a nanocomposite.

All results accounted, it is evident that increased proportions of MoS_2 (1:2 and 1:5) in PANI/MoS_2 yields enhanced anti-amoebic effects compared to 1:1 ratio across genera. Although the anti-parasitic potential of TMDC-based polymer nanocomposite is a novel aspect, high antibacterial activities of MoS_2-based nanoflowers toward Gram-positive and Gram-negative multi-drug resistant bacteria have been recognized.[31b] The mechanism of microbial inhibition employed by MoS_2- and PANI-based nanomaterials is yet to be understood extensively. However, effective antimicrobial effects have been studied to be the result of a combination of oxidative stress, membrane damage, as well as metabolic inactivation.[20b,36] Essentially, oxidative stress generation is either dependent on the ROS produced by the nanostructure or ROS-independent, following the disruption or oxidation of a cellular component, in turn affecting a vital biological process.[37] Oxidative stress induced in microbial treatment with nanocomposites of MoS_2 has been attributed to ROS-dependent[21,38] as well as ROS-independent pathways.[39]

PANI/MoS_2 Induced Intracellular ROS Production in *A. castellanii* Trophozoites. Due to the congruous 2D planar structure of MoS_2 and graphene materials, it has been suggested that these analogues may employ comparable methods in inhibiting microbial viability including ROS generation and contact-induced membrane stress. To establish an understanding of the mechanism of the action of PANI/MoS_2 in inhibiting *A. castellanii* trophozoites, ROS generation was examined. For this, 2′,7′-dichlorofluorescein diacetate (DCFDA) reagent (Sigma-Aldrich) was employed. In the cytoplasm of trophozoites, cellular esterases cleave the lipophilic groups off this cell-permeable reagent, rendering H_2DCF. The presence of intracellular ROS oxidizes H_2DCF into a highly fluorescent DCF, detected microscopically and used as a marker of ROS levels. In this study, untreated *A.*

https://doi.org/10.1021/acsomega.2c06050
ACS Omega 2023, 8, 8237−8247

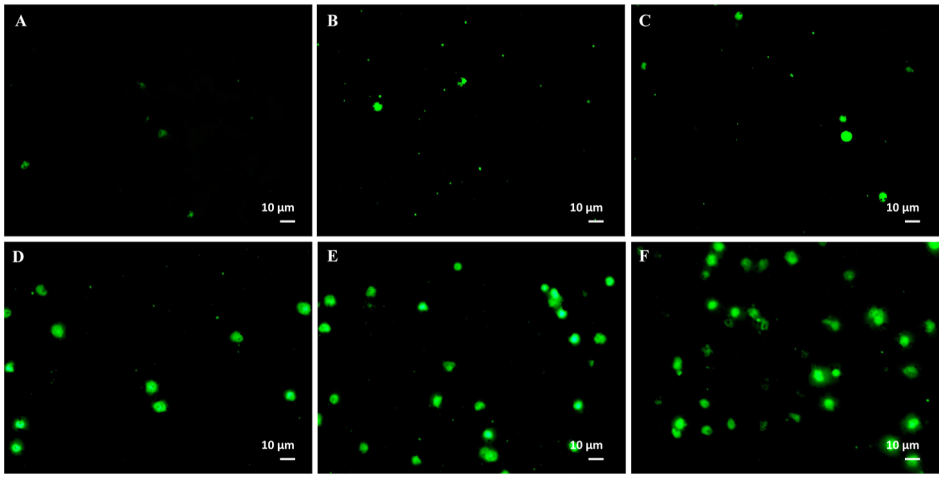

Figure 6. Fluorescence microscopy images representing the generation of intracellular ROS in *A. castellanii* as a result of treatment with up to 100 μg/mL PANI/MoS_2 (1:1, 1:2, and 1:5) and controls (PANI alone and MoS_2 alone). Briefly, PANI/MoS_2 and controls were incubated with *A. castellanii* trophozoites for 24 h at 30 °C. ROS production was determined by staining with DCF-DA reagent, and the intensity of DCF fluorescence was visualized as proportional to ROS levels with fluorescence microscopy. (A) Untreated amoeba (negative control); (B) 50 μg/mL PANI control; (C) 83.3 μg/mL MoS_2 control; (D) 100 μg/mL PANI/MoS_2 (1:1); (E) 100 μg/mL PANI/MoS_2 (1:2); (F) 100 μg/mL PANI/MoS_2 (1:5).

castellanii and amoeba treated with 100 μg/mL PANI/MoS_2 at three ratios (1:1, 1:2, and 1:5) were assayed for intracellular ROS. The visible levels of ROS generated in amoeba treated with PANI alone and MoS_2 alone were also explored. The fluorescence intensity, proportional to intracellular ROS, that was captured from PANI/MoS_2-treated amoeba was noticeably increased relative to the untreated amoeba. ROS levels were increased with increasing MoS_2 dimension of the nanocomposite in the 1:2 and 1:5 ratios of PANI/MoS_2. However, all three ratios of the composite, PANI/MoS_2, demonstrated higher fluorescence levels relative to individual components (PANI alone and MoS_2 alone) (Figure 6).

As noted previously, our findings of ROS-dependent inhibition of *A. castellanii* viability are consistent with the use of MoS_2-polymer-based nanomaterials for the treatment of other microorganisms.[21,36] It was reported that increased microbial ROS generation was detected with MoS_2 nanoplatforms in comparison to graphene analogues. The production of ROS, in addition to the formation of free radicals as well as Mo^{4+} ion release,[40] due to MoS_2 nanocomposite treatment, would upsurge oxidative stress. Excessive ROS production is notorious for causing DNA fragmentation as well as eliciting damage to other cellular components including the membrane.[41] Consequently, the microbial structural integrity is compromised, intracellular components leak out, and microbial death ensues.

Field Emission Scanning Electron Microscopy Analysis of *A. castellanii* after Treatment with PANI/MoS_2. A larger grasp of the mode of *A. castellanii* inhibition ensuing treatment with PANI/MoS_2 was established ultrastructurally through field emission—scanning electron microscopic analysis. For this, the 1:5 ratio of 100 μg/mL PANI/MoS_2 was used for its relatively superior amoebicidal capacity. Spine-like, slender protrusions were pictured throughout the surface of untreated *A. castellanii* (negative control) and identified as its characteristic acanthopodia (Figure 7). In comparison, treating amoeba with PANI/MoS_2 (1:5) generated visible sunken pores and blebs on the *A. castellanii* surface. Further, the overall disruption of the amoeba membrane was visualized in treated

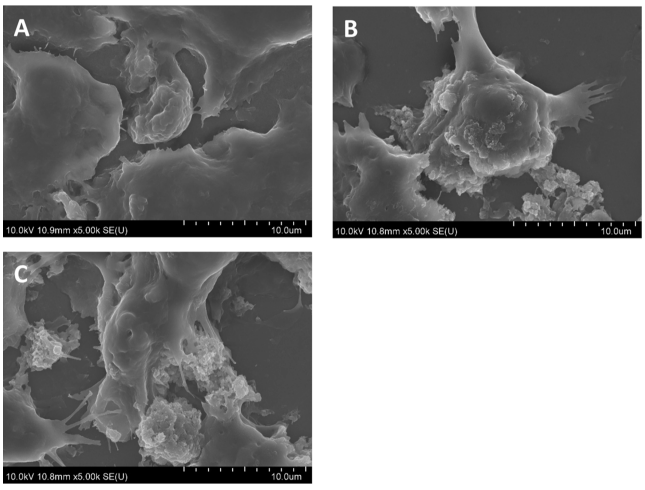

Figure 7. Field-emission scanning electron micrographs (FE-SEM) portraying (A) untreated *A. castellanii* and (B,C) *A. castellanii* treated with 100 μg/mL PANI/MoS_2 (1:5). Subsequent to treatment, amoeba was fixed with 2.5% glutaraldehyde onto glass coverslips which were sequentially dehydrated with a succession of ethanol washes. Samples were then air-dried and sputtered in platinum preceding imaging on the FE-SEM Hitachi SU8010 instrument. Untreated *A. castellanii* was pictured with representative acanthopodia on the surface of consistent amoeboid morphology, in contrast to the evidently disrupted structure of nanocomposite-treated amoeba.

amoeba, which has been noted to distinctly affect the cytolytic mechanism of the parasite—a key factor in its pathogenicity. Thus, the *A. castellanii* inhibition activity of 100 μg/mL of PANI/MoS_2 can be comprehended to be the result of these morphological disturbances that are likely contact-induced or ROS-mediated as aforementioned.

CONCLUSIONS

In summary, the findings in this study represent the novel antiamoebic activities of PANI/MoS_2 nanocomposite toward two genera of brain-eating amoebae, namely *Naegleria* and *Acanthamoeba*. Against both trophozoite and cyst life stages

https://doi.org/10.1021/acsomega.2c06050
ACS Omega 2023, 8, 8237−8247

of *A. castellanii* and *N. fowleri*, the nanocomposite formulated with increased proportions of MoS_2 (1:2 and 1:5) was noted to be superior. This treatment was studied to generate intracellular ROS which would increase oxidative stress and possibly inhibit amoebae through DNA damage or membrane disruptions as visualized as ultrastructural morphological alterations through FE-SEM. Further, PANI/MoS_2 displayed limited cytotoxic effects toward human cell lines—HaCaT and pHCEC. These positive outcomes necessitate further evaluation of the mechanism of inhibition as well as the in vivo behavior of PANI/MoS_2 for its practical application as chemotherapeutic agent against the devastating CNS infections due to brain-eating amoebae.

METHODS

Chemicals. All chemicals used in this study were purchased from Sigma-Aldrich (San Francisco, CA, USA) unless stated otherwise. HPLC-grade organic solvents were obtained from Fisher Scientific (UK) for use in the synthesis and purification of nanomaterials. Aniline (Fluka, ≥99%) was distilled under reduced pressure; then, it was stored in the dark for later use. Without additional purification, 37% hydrochloric acid (HCl), ammonium persulfate (APS; 37%), acetone, and methanol were purchased from Merck (Darmstadt, Germany). MoS_2 powder was purchased from Lowe Friction Company (Canada). The average particle size of the powder was 70 nm.

Preparation of PANI Nanotubes. Distilled aniline was added to 1 M HCl solution in order to prepare PANI nanotubes via the oxidative polymerization method, with APS serving as the oxidant. 30 mL of a 1 M HCl aqueous solution was used added to 0.0215 mol of aniline. At 0−5 °C with continuous stirring, APS was added dropwise into the aniline solution. To complete the polymerization, the solution was stirred for 3 h and then kept in refrigerator to obtain the desired mixture. Following this, the mixture was put through filtration and rinsed with 0.5 M HCl till the filtrate became colorless and then with deionized water till the filtrate became neutral. Thereafter, in order to eliminate unreacted oligomers and monomers, the obtained polymer product was rinsed with 1:1 solvent mixture of methanol and acetone. The product was oven-dried overnight at a temperature of 60 °C and pressure of 100 mb. The resulting polymer product's appearance as a green color indicated the successful preparation of conductive PANI emeraldine salt.

Preparation of PANI/MoS_2 Nanocomposite. To prepare the nanocomposites of PANI/MoS_2 nanosheets, 1, 2, and 5 weight % of MoS_2 with regard to 0.0215 mol of aniline were taken. In 5 mL of deionized water, an estimated quantity of MoS_2 was added under sonication. Then, this mixture was drop by drop added to aniline solution containing HCl under vigorous stirring. To obtain a homogeneous solution, the resulting mixture was sonicated for some more time. The workup process followed the same procedure as mentioned in the section above. The resulting nanocomposites were given the codes P−MoS_2-1, P−MoS_2-2, and P−MoS_2-5, denoting the 1, 2, and 5 weight % of MoS_2 nanosheets relative to aniline.

Characterization of PANI/MoS_2. The FE-SEM images were captured using the JEOL JSM-7600F model with an accelerator voltage of 10 kV to determine the elemental analysis and the surface morphology of the prepared nanocomposites. The TEM images were taken using the JEOL JEM-2100F model to determine the crystallinity, shape, and size of the prepared products.

***A. castellanii* Cultures.** *A. castellanii* (ATCC 50492) of T4 genotype was acquired from American Type Culture Collection (ATCC) and cultured with PYG growth media constituting 0.75% w/v of proteose peptone, 0.75% w/v of yeast extract, and 1.5% w/v of D-glucose in 75 cm^2 culture flasks incubated at 30 °C. To obtain healthy *A. castellanii* trophozoites for use in assays, flasks were placed on ice for 10 min prior to gentle tapping to detach adherent cells. The cell suspension was then transferred into a falcon tube and centrifuged at 3,000 rpm for 10 min to obtain a cell pellet. The pellet was then resuspended in Rosewell Park Memorial Institute (RPMI-1640) media, and cells were enumerated using a hemocytometer as previously presented.[42] *A. castellanii* cysts were prepared by incubating trophozoites on non-nutrient bacteriological agar (1.5% w/v) for up to 2 weeks with routine microscopic evaluation until the emergence of mature cysts was observed. Cysts were then obtained by scraping the agar using a cell lifter and phosphate buffered saline (PBS) before counting with a hemocytometer for use in cysticidal assays.

***N. fowleri* Culture.** Procured from ATCC, the *N. fowleri* cells (HBI strain, ATCC 30174) used in this study were originally obtained from the CNS of a PAM patient. *N. fowleri* trophozoites were cultivated in RPMI-1640 media in 75 cm^2 flasks with a confluent feeder layer of Henrietta Lacks cervical adenocarcinoma cells (HeLa). The media was supplemented with 1% penicillin−streptomycin (Nacalai Tesque, Japan) and incubated at 37 °C supplied with 5% CO_2 until the complete consumption of HeLa cells was visualized microscopically. To obtain trophozoites for use in experiments, flasks were tapped, and the cell suspension was centrifuged at 1258*g* for 5 min. The obtained cell pellet was resuspended in RPMI-1640, and trophozoites were counted with a hemocytometer. *N. fowleri* cysts were cultured by transferring the trophozoites into a new flask in RPMI-1640 after their complete ingestion of the HeLa layer. Cells were microscopically examined routinely for the formation of mature cysts that were acquired for cysticidal assays in the same manner described.[43]

Henrietta Lacks Cervical Adenocarcinoma Cells (HeLa). HeLa cells (ATCC CCL-2) were obtained from ATCC and cultured for feeding *N. fowleri*. In HeLa cultures, RPMI-1640 media (Serana, Germany) was complemented with 1% minimum essential media non-essential amino acids (MEM NEAA), 1% L-glutamine, 1% penicillin streptomycin antibiotic, and 10% foetal bovine serum (FBS) utilized in flasks incubated at 37 °C with a supply of CO_2 (5%) and humidity (95%). Upon reaching confluency, as visualized microscopically, trypsin was used to detach the cells, and the cell suspension was transferred into a falcon tube and centrifuged at 1258*g* for 5 min. The pellet obtained was resuspended in RPMI-1640 and seeded into flasks for further use or plates for experimental observation.[44]

Cultures of Human Keratinocyte Skin Cell (HaCaT). Human Keratinocyte skin cells (CVCL_0038 and CLS: 300493) were acquired from Cell Lines Services (CLS, Germany). For HaCaT culture, RPMI-1640 media (Serana, Germany) was used complemented with 1% MEM NEAA, 1% L-glutamine, 1% penicillin streptomycin antibiotic, and 10% FBS in 75 cm^2 culture flasks in a humidified 37 °C incubator with 5% CO_2. To detach the adherent HaCaT cells to be used in cytotoxicity assays, trypsin was added to cells. HaCaT cells were then seeded in 96-well plates and incubated at 37 °C for 24 h or until a monolayer was observed.[45]

https://doi.org/10.1021/acsomega.2c06050
ACS Omega 2023, 8, 8237−8247

Primary Corneal Epithelial Cell Culture. pHCEC (ATCC PCS-700-010) were obtained from American Type Culture Collection (ATCC) and cultured following the ATCC-recommended protocol. pHCEC was cultured in tissue flasks with Corneal Epithelial Cell Basal Medium (ATCC PCS-700-030) supplemented with the final concentrations of 5 μg/mL apo-transferrin, 5 μg/mL rh insulin, 100 ng/mL hydrocortisone hemisuccinate, 1 μM epinephrine, 6 mM L-glutamine, and 0.4% extract P and CE growth factors (ATCC) and incubated at 37 °C with a supply of 5% CO_2. Trypsin−EDTA was used to detach the pHCEC, and the cell suspension was centrifuged at 150*g* for 5 min before seeding into flasks or well-plates and observed until confluency was achieved.

Amoebicidal Assays. Amoebicidal assays were performed to assess the effects of PANI/MoS_2 on *A. castellanii* and *N. fowleri* trophozoite viability. In short, 2.5 × 10^5 trophozoites were incubated in RPMI-1640 with three ratios (1:1, 1:2, and 1:5) of PANI/MoS_2 at 100 μg/mL for 24 h at 30 °C. *A. castellanii* positive control (chlorhexidine gluconate) and *N. fowleri* positive control (miltefosine) were also tested alongside negative controls and component controls at ratio-respective concentrations (PANI alone and MoS_2 alone). After 24 h, trypan blue (0.1%) exclusion assays were conducted wherein live cells were distinguished from stained dead cells allowing their enumeration using a haemocytometer.[46]

Assessment of Cysticidal Activity. Cysts of *A. castellanii* and *N. fowleri* were cultured as aforementioned for cysticidal assays. 2.5 × 10^5 cysts were treated with 100 μg/mL of PANI/MoS_2 at three ratios (1:1, 1:2, and 1:5), PANI alone, MoS_2 alone, as well as negative and positive controls in RPMI-1640 for 24 h at 30 °C. Subsequent to the incubation time, 0.1% trypan blue was used to differentiate unstained live cysts for counting using a hemocytometer.[47]

LDH Cytotoxicity Assays. The host cell cytotoxic effects of PANI/MoS_2 were evaluated in LDH cytotoxicity assays. Briefly, PANI/MoS_2 (100 μg/mL) was added to monolayers of HaCaT and pHCEC in 96-well plates and incubated at 37 °C, 5% CO_2 for 24 h. After the incubation time, cells allocated for the positive control were treated with 0.2% Triton X-100 for 30 min. Subsequently, supernatant from each well was transferred into a new 96-well plate, and an equal volume of LDH kit reagent (Roche) was added. After 10 min in the dark, the absorbance was measured at 490 nm using a spectrophotometric plate reader. Percentage cytotoxicity was calculated as described previously.[48]

ROS Assays. DCFDA reagent (Sigma-Aldrich, San Francisco, USA) was used to study the ROS in *A. castellanii* trophozoites treated with PANI/MoS_2. 2.5 × 10^5 *A. castellanii* trophozoites were treated with 1:1, 1:2, and 1:5 PANI/MoS_2 at 100 μg/mL in RPMI-1640 as described for amoebicidal assays. After 24 h incubation at 30 °C, PBS was used to double wash trophozoites before the DCFDA reagent was added to the cells at a final well concentration of 25 μM in RPMI-1640. The cells were incubated with the reagent for 45 min in the dark and afterward washed with PBS once again. Images were recorded using the fluorescence microscope.[49]

Field-Emission Scanning Electron Microscopy. FE-SEM was employed to visualize the structural and morphological changes to *A. castellanii* trophozoites' surface before and after treatment with PANI/MoS_2. 100 μg/mL of PANI/MoS_2 at 1:5 ratio was utilized in the analysis for its promising amoebicidal capacity. After treatment for 6 h, 2.5% glutaraldehyde was used to fix trophozoites onto glass cover slips. To achieve complete infiltration, trophozoites were incubated in glutaraldehyde for 2 h. After fixation, dehydration of the samples was achieved with ethanol solutions (50−100%). Samples were sputtered with platinum before visualizing under an FE-SEM instrument (Hitachi SU8010).[50]

Statistical Analysis. The data presented is representative of the mean ± standard error of several individual experiments, each performed in duplicates. Two-sample *t*-tests, with two-tailed distribution comparing the means of independent experiments, were employed to calculate the *P* value and, in turn, determine statistical significance.

■ ETHICAL APPROVAL

Animal and/or human studies were not performed.

■ AUTHOR INFORMATION

Corresponding Authors

Syed Shahabuddin − *Department of Chemistry, School of Energy Technology, Pandit Deendayal Energy University, Raisan, Gandhinagar 382426, India; Faculty of Applied Sciences, Universiti Teknologi MARA, Shah Alam 40450, Malaysia*; Email: syed.shahabuddin@sot.pdpu.ac.in

Ayaz Anwar − *Department of Biological Sciences, School of Medical and Life Sciences, Sunway University, Subang Jaya 47500 Selangor, Malaysia*; orcid.org/0000-0001-8638-3193; Phone: +603-74918622 Ext. 7174; Email: ayazanwarkk@yahoo.com; Fax: +603-56358630

Authors

Sumayah Abdelnasir − *Department of Biological Sciences, School of Medical and Life Sciences, Sunway University, Subang Jaya 47500 Selangor, Malaysia*

Mohammad Ridwane Mungroo − *Department of Medical Biology, Amsterdam Cardiovascular Sciences, Amsterdam University Medical Centre, Amsterdam 1105 AZ, The Netherlands*

Jactty Chew − *Department of Biological Sciences, School of Medical and Life Sciences, Sunway University, Subang Jaya 47500 Selangor, Malaysia*

Ruqaiyyah Siddiqui − *Department of Biology, Chemistry and Environmental Sciences, College of Arts and Sciences, American University of Sharjah, Sharjah 26666, United Arab Emirates; Faculty of Medicine, Istinye University, Istanbul 34010, Turkey*

Naveed Ahmed Khan − *Department of Clinical Sciences, College of Medicine, University of Sharjah, Sharjah 27272, United Arab Emirates; Department of Medical Biology, Faculty of Medicine, Istinye University, Istanbul 34010, Turkey*; orcid.org/0000-0001-7667-8553

Irfan Ahmad − *Department of Clinical Laboratory Sciences, College of Applied Medical Sciences, King Khalid University, Abha 62529, Saudi Arabia*

Complete contact information is available at: https://pubs.acs.org/10.1021/acsomega.2c06050

Author Contributions

The study was conceptualized by A.A. and N.A.K. I.A. and J.C. acquired funding and supervised the entire study. S.S. synthesized and characterized the materials. All experiments were carried out by S.A. and M.R.M. under the supervision of A.A. and R.S. S.A. drafted the full manuscript. All authors edited and approved the final manuscript.

https://doi.org/10.1021/acsomega.2c06050
ACS Omega 2023, 8, 8237−8247

Funding

The work was supported by the Ministry of Higher Education Malaysia (FRGS/1/2018/SKK08/SYUC/01/1). The authors also acknowledge the Scientific Research Deanship at King Khalid University for their support through the Large Research Group Project (RGP.02/186/-43).

Notes

The authors declare no competing financial interest.
Data will be provided upon request on a case-to-case basis.

■ ACKNOWLEDGMENTS

Authors would like to thank Sunway University for their support.

■ REFERENCES

(1) Król-Turmińska, K.; Olender, A. Human infections caused by free-living amoebae. *Ann. Agric. Environ. Med.* **2017**, *24*, 254−260.
(2) Taravaud, A.; Fechtali-Moute, Z.; Loiseau, P. M.; Pomel, S. Drugs used for the treatment of cerebral and disseminated infections caused by free-living amoebae. *Clin. Transl. Sci.* **2021**, *14*, 791−805.
(3) Schuster, F. L.; Visvesvara, G. S. Free-living amoebae as opportunistic and non-opportunistic pathogens of humans and animals. *Int. J. Parasitol.* **2004**, *34*, 1001−1027.
(4) (a) Saberi, R.; Seifi, Z.; Dodangeh, S.; Najafi, A.; Abdollah Hosseini, S.; Anvari, D.; Taghipour, A.; Norouzi, M.; Niyyati, M. A systematic literature review and meta-analysis on the global prevalence of *Naegleria* spp. in water sources. *Transboundary Emerging Dis.* **2020**, *67*, 2389−2402. (b) Cope, J. R.; Ali, I. K. Primary amebic meningoencephalitis: what have we learned in the last 5 years? *Curr. Infect. Dis. Rep.* **2016**, *18*, 31.
(5) (a) Siddiqui, R.; Khan, N. A. Primary amoebic meningoencephalitis caused by *Naegleria fowleri*: an old enemy presenting new challenges. *PLoS Neglected Trop. Dis.* **2014**, *8*, No. e3017. (b) Siddiqui, R.; Ali, I. K. M.; Cope, J. R.; Khan, N. A. Biology and pathogenesis of *Naegleria fowleri*. *Acta Trop.* **2016**, *164*, 375−394.
(6) Pana, A.; Vijayan, V.; Anilkumar, A. C. *Amebic meningoencephalitis*; StatPearls, 2017.
(7) Khan, N. A. *Acanthamoeba*: biology and increasing importance in human health. *FEMS Microbiol. Rev.* **2006**, *30*, 564−595.
(8) (a) Siddiqui, R.; Khan, N. A. Biology and pathogenesis of *Acanthamoeba*. *Parasites Vectors* **2012**, *5*, 6. (b) Maciver, S. K.; Asif, M.; Simmen, M. W.; Lorenzo-Morales, J. A systematic analysis of *Acanthamoeba* genotype frequency correlated with source and pathogenicity: T4 is confirmed as a pathogen-rich genotype. *Eur. J. Protistol.* **2013**, *49*, 217−221.
(9) (a) Visvesvara, G. S.; Moura, H.; Schuster, F. L. Pathogenic and opportunistic free-living amoebae: *Acanthamoeba* spp., *Balamuthia mandrillaris*, *Naegleria fowleri*, and *Sappinia diploidea*. *FEMS Immunol. Med. Microbiol.* **2007**, *50*, 1−26. (b) Elsheikha, H. M.; Siddiqui, R.; Khan, N. A. Drug Discovery against *Acanthamoeba* Infections: Present Knowledge and Unmet Needs. *Pathogens* **2020**, *9*, 405.
(10) Kim, J.-H.; Jung, S.-Y.; Lee, Y.-J.; Song, K.-J.; Kwon, D.; Kim, K.; Park, S.; Im, K.-I.; Shin, H.-J. Effect of therapeutic chemical agents in vitro and on experimental meningoencephalitis due to *Naegleria fowleri*. *Antimicrob. Agents Chemother.* **2008**, *52*, 4010−4016.
(11) (a) Mungroo, M. R.; Anwar, A.; Khan, N. A.; Siddiqui, R. Brain-eating amoebae infection: Challenges and opportunities in chemotherapy. *Mini-Rev. Med. Chem.* **2019**, *19*, 980−987. (b) Pervin, N.; Sundareshan, V. *Naegleria*; StatPearls, 2020.
(12) Grace, E.; Asbill, S.; Virga, K. *Naegleria fowleri*: pathogenesis, diagnosis, and treatment options. *Antimicrob. Agents Chemother.* **2015**, *59*, 6677−6681.
(13) Duggal, S. D.; Rongpharpi, S.; Duggal, A.; Kumar, A.; Biswal, I. Role of *Acanthamoeba* in granulomatous encephalitis: a review. *J. Infect. Dis. Ther.* **2017**, *1*, 1.
(14) Kalra, S. K.; Sharma, P.; Shyam, K.; Tejan, N.; Ghoshal, U. *Acanthamoeba* and its pathogenic role in granulomatous amebic encephalitis. *Exp. Parasitol.* **2020**, *208*, 107788.
(15) (a) Sharma, G.; Kalra, S. K.; Tejan, N.; Ghoshal, U. Nanoparticles based therapeutic efficacy against *Acanthamoeba*: Updates and future prospect. *Exp. Parasitol.* **2020**, *218*, 108008. (b) Vimbela, G. V.; Ngo, S. M.; Fraze, C.; Yang, L.; Stout, D. A. Antibacterial properties and toxicity from metallic nanomaterials. *Int. J. Nanomed.* **2017**, *12*, 3941−3965.
(16) (a) Hoseinzadeh, E.; Makhdoumi, P.; Taha, P.; Hossini, H.; Stelling, J.; Kamal, M. A.; Ashraf, G. M. A review on nano-antimicrobials: metal nanoparticles, methods and mechanisms. *Curr. Drug Metab.* **2017**, *18*, 120−128. (b) Kalwar, K.; Shan, D. Antimicrobial effect of silver nanoparticles (AgNPs) and their mechanism − a mini review. *Micro Nano Lett.* **2018**, *13*, 277−280.
(17) Wang, L.; Hu, C.; Shao, L. The antimicrobial activity of nanoparticles: present situation and prospects for the future. *Int. J. Nanomed.* **2017**, *12*, 1227.
(18) Tan, C.; Lai, Z.; Zhang, H. Ultrathin Two-Dimensional Multinary Layered Metal Chalcogenide Nanomaterials. *Adv. Mater.* **2017**, *29*, 1701392.
(19) Zheng, Y.; Hong, X.; Wang, J.; Feng, L.; Fan, T.; Guo, R.; Zhang, H. 2D Nanomaterials for Tissue Engineering and Regenerative Nanomedicines: Recent Advances and Future Challenges. *Adv. Healthcare Mater.* **2021**, *10*, 2001743.
(20) (a) Cai, S.; Yang, R. Two-Dimensional Nanomaterials With Enzyme-Like Properties for Biomedical Applications. *Front. Chem.* **2020**, *8*, 565940. (b) Agarwal, V.; Chatterjee, K. Recent advances in the field of transition metal dichalcogenides for biomedical applications. *Nanoscale* **2018**, *10*, 16365−16397.
(21) Cao, W.; Yue, L.; Wang, Z. High antibacterial activity of chitosan—molybdenum disulfide nanocomposite. *Carbohydr. Polym.* **2019**, *215*, 226−234.
(22) Teo, W. Z.; Chng, E. L. K.; Sofer, Z.; Pumera, M. Cytotoxicity of exfoliated transition-metal dichalcogenides (MoS_2, WS_2, and WSe_2) is lower than that of graphene and its analogues. *Chem. Eur. J.* **2014**, *20*, 9627−9632.
(23) Appel, J. H.; Li, D. O.; Podlevsky, J. D.; Debnath, A.; Green, A. A.; Wang, Q. H.; Chae, J. Low Cytotoxicity and Genotoxicity of Two-Dimensional MoS_2 and WS_2. *ACS Biomater. Sci. Eng.* **2016**, *2*, 361−367.
(24) Wang, Y.; Ma, Y.; Shi, J.; Yan, X.; Luo, J.; Zhu, H.; Jia, K.; Li, J.; Zhang, C. Y. Surface Modification of Monolayer MoS_2 by Baking for Biomedical Applications. *Front. Chem.* **2020**, *8*, 741.
(25) (a) Feng, X.; Wang, X.; Xing, W.; Zhou, K.; Song, L.; Hu, Y. Liquid-exfoliated MoS_2 by chitosan and enhanced mechanical and thermal properties of chitosan/MoS_2 composites. *Compos. Sci. Technol.* **2014**, *93*, 76−82. (b) Thakur, S.; Bandyopadhyay, P.; Kim, S. H.; Kim, N. H.; Lee, J. H. Enhanced physical properties of two dimensional MoS_2/poly(vinyl alcohol) nanocomposites. *Composites A* **2018**, *110*, 284−293.
(26) (a) Moghadam, P. N.; Zareh, E. N. Synthesis of conductive nanocomposites based on polyaniline/poly (styrene-alt-maleic anhydride)/polystyrene. *e-Polymers* **2010**, *10*, 054, DOI: 10.1515/epoly.2010.10.1.588. (b) Kiristi, M.; Uygun, A. Polyaniline. *Handbook of Engineering and Specialty Thermoplastics*; John Wiley & Sons, 2011; Vol *4*, pp 183−210.
(27) (a) Zare, E. N.; Makvandi, P.; Ashtari, B.; Rossi, F.; Motahari, A.; Perale, G. Progress in conductive polyaniline-based nanocomposites for biomedical applications: a review. *J. Med. Chem.* **2019**, *63*, 1−22. (b) Abdelnasir, S.; Anwar, A.; Anwar, A. Conducting Polymer-Based Nanocomposites Against Pathogenic Bacteria. *Advances in Hybrid Conducting Polymer Technology*; Springer, 2021, pp 271−310.
(28) (a) Lalegül-Ülker, Ö.; Elçin, A. E.; Elçin, Y. M. Intrinsically conductive polymer nanocomposites for cellular applications. *Adv. Exp. Med. Biol.* **2018**, 135−153. (b) Giliopoulos, D.; Zamboulis, A.; Giannakoudakis, D.; Bikiaris, D.; Triantafyllidis, K. Polymer/metal

organic framework (MOF) nanocomposites for biomedical applications. *Molecules* **2020**, *25*, 185.
(29) (a) Humpolicek, P.; Kasparkova, V.; Saha, P.; Stejskal, J. Biocompatibility of polyaniline. *Synth. Met.* **2012**, *162*, 722−727. (b) Wang, C. H.; Dong, Y.; Sengothi, K.; Tan, K.; Kang, E. In-vivo tissue response to polyaniline. *Synth. Met.* **1999**, *102*, 1313−1314.
(30) (a) Abdelnasir, S.; Mungroo, M. R.; Shahabuddin, S.; Siddiqui, R.; Khan, N. A.; Anwar, A. Polyaniline-conjugated boron nitride nanoparticles exhibiting potent effects against pathogenic brain-eating amoebae. *ACS Chem. Neurosci.* **2021**, *12*, 3579−3587. (b) Abdelnasir, S.; Mungroo, M. R.; Shahabuddin, S.; Siddiqui, R.; Khan, N. A.; Ahmad, I.; Anwar, A. Polyaniline (PANI)-conjugated tungsten disulphide (WS_2) nanoparticles as potential therapeutics against brain-eating amoebae. *Appl. Microbiol. Biotechnol.* **2022**, *106*, 3279−3291.
(31) (a) Shang, E.; Niu, J.; Li, Y.; Zhou, Y.; Crittenden, J. C. Comparative toxicity of Cd, Mo, and W sulphide nanomaterials toward *E. coli* under UV irradiation. *Environ. Pollut.* **2017**, *224*, 606−614. (b) Yin, W.; Yu, J.; Lv, F.; Yan, L.; Zheng, L. R.; Gu, Z.; Zhao, Y. Functionalized Nano-MoS(2) with Peroxidase Catalytic and Near-Infrared Photothermal Activities for Safe and Synergetic Wound Antibacterial Applications. *ACS Nano* **2016**, *10*, 11000−11011. (c) Wu, N.; Yu, Y.; Li, T.; Ji, X.; Jiang, L.; Zong, J.; Huang, H. Investigating the influence of MoS_2 nanosheets on *E. coli* from metabolomics level. *PLoS One* **2016**, *11*, No. e0167245.
(32) (a) Youssef, A. M.; Moustafa, H. A.; Barhoum, A.; Hakim, A. E. F. A. A.; Dufresne, A. Evaluation of the Morphological, Electrical and Antibacterial Properties of Polyaniline Nanocomposite Based on Zn/Al-Layered Double Hydroxides. *ChemistrySelect* **2017**, *2*, 8553−8566. (b) Liang, X.; Govindaraju, S.; Yun, K. Dual applicability of polyaniline coated gold nanorods: a study of antibacterial and redox activity. *BioChip J.* **2018**, *12*, 137−145. (c) Hou, Y.; Feng, J.; Wang, Y.; Li, L. Enhanced antibacterial activity of Ag-doped ZnO/polyaniline nanocomposites. *J. Mater. Sci.: Mater. Electron.* **2016**, *27*, 6615−6622.
(33) Fan, J.; Li, Y.; Nguyen, H. N.; Yao, Y.; Rodrigues, D. F. Toxicity of exfoliated-MoS_2 and annealed exfoliated-MoS_2 towards planktonic cells, biofilms, and mammalian cells in the presence of electron donor. *Environ. Sci.: Nano* **2015**, *2*, 370−379.
(34) Mukheem, A.; Shahabuddin, S.; Akbar, N.; Anwar, A.; Sarih, N. M.; Sudesh, K.; Khan, N. A.; Sridewi, N. Fabrication of biopolymer polyhydroxyalkanoate/chitosan and 2D molybdenum disulfide−doped scaffolds for antibacterial and biomedical applications. *Appl. Microbiol. Biotechnol.* **2020**, *104*, 3121−3131.
(35) Hao, J.; Song, G.; Liu, T.; Yi, X.; Yang, K.; Cheng, L.; Liu, Z. In Vivo Long-Term Biodistribution, Excretion, and Toxicology of PEGylated Transition-Metal Dichalcogenides MS(2) (M = Mo, W, Ti) Nanosheets. *Adv. Sci.* **2017**, *4*, 1600160.
(36) Kasinathan, K.; Marimuthu, K.; Murugesan, B.; Samayanan, S.; Panchu, S. J.; Swart, H. C.; Savariroyan, S. R. I. Synthesis of biocompatible chitosan functionalized Ag decorated biocomposite for effective antibacterial and anticancer activity. *Int. J. Biol. Macromol.* **2021**, *178*, 270−282.
(37) Begum, S.; Pramanik, A.; Davis, D.; Patibandla, S.; Gates, K.; Gao, Y.; Ray, P. C. 2D and Heterostructure Nanomaterial Based Strategies for Combating Drug-Resistant Bacteria. *ACS Omega* **2020**, *5*, 3116−3130.
(38) Yang, X.; Li, J.; Liang, T.; Ma, C.; Zhang, Y.; Chen, H.; Hanagata, N.; Su, H.; Xu, M. Antibacterial activity of two-dimensional MoS_2 sheets. *Nanoscale* **2014**, *6*, 10126−10133.
(39) Pandit, S.; Karunakaran, S.; Boda, S. K.; Basu, B.; De, M. High Antibacterial Activity of Functionalized Chemically Exfoliated MoS_2. *ACS Appl. Mater. Interfaces* **2016**, *8*, 31567−31573.
(40) Roy, S.; Mondal, A.; Yadav, V.; Sarkar, A.; Banerjee, R.; Sanpui, P.; Jaiswal, A. Mechanistic Insight into the Antibacterial Activity of Chitosan Exfoliated MoS2 Nanosheets: Membrane Damage, Metabolic Inactivation, and Oxidative Stress. *ACS Appl. Bio Mater.* **2019**, *2*, 2738−2755.
(41) Banerjee, M.; Mallick, S.; Paul, A.; Chattopadhyay, A.; Ghosh, S. S. Heightened Reactive Oxygen Species Generation in the Antimicrobial Activity of a Three Component Iodinated Chitosan−Silver Nanoparticle Composite. *Langmuir* **2010**, *26*, 5901−5908.
(42) Sissons, J.; Alsam, S.; Stins, M.; Rivas, A. O.; Morales, J. L.; Faull, J.; Khan, N. A. Use of in vitro assays to determine effects of human serum on biological characteristics of *Acanthamoeba castellanii*. *J. Clin. Microbiol.* **2006**, *44*, 2595−2600.
(43) Rajendran, K.; Anwar, A.; Khan, N. A.; Shah, M. R.; Siddiqui, R. trans-Cinnamic acid conjugated gold nanoparticles as potent therapeutics against brain-eating amoeba *Naegleria fowleri*. *ACS Chem. Neurosci.* **2019**, *10*, 2692−2696.
(44) Rajendran, K.; Anwar, A.; Khan, N. A.; Siddiqui, R. Brain-eating amoebae: silver nanoparticle conjugation enhanced efficacy of anti-amoebic drugs against *Naegleria fowleri*. *ACS Chem. Neurosci.* **2017**, *8*, 2626−2630.
(45) Siddiqui, R.; Jeyamogan, S.; Ali, S. M.; Abbas, F.; Sagathevan, K.; Khan, N. A. Crocodiles and alligators: Antiamoebic and antitumor compounds of crocodiles. *Exp. Parasitol.* **2017**, *183*, 194−200.
(46) Lakhundi, S.; Khan, N. A.; Siddiqui, R. Inefficacy of marketed contact lens disinfection solutions against keratitis-causing *Acanthamoeba castellanii* belonging to the T4 genotype. *Exp. Parasitol.* **2014**, *141*, 122−128.
(47) Abdelnasir, S.; Anwar, A.; Kawish, M.; Anwar, A.; Shah, M. R.; Siddiqui, R.; Khan, N. A. Metronidazole conjugated magnetic nanoparticles loaded with amphotericin B exhibited potent effects against pathogenic *Acanthamoeba castellanii* belonging to the T4 genotype. *AMB Express* **2020**, *10*, 127.
(48) Anwar, A.; Mungroo, M. R.; Anwar, A.; Sullivan, W. J., Jr; Khan, N. A.; Siddiqui, R. Repositioning of guanabenz in conjugation with gold and silver nanoparticles against pathogenic amoebae *Acanthamoeba castellanii* and *Naegleria fowleri*. *ACS Infect. Dis.* **2019**, *5*, 2039−2046.
(49) Jha, B. K.; Jung, H.-J.; Seo, I.; Suh, S.-I.; Suh, M.-H.; Baek, W.-K. Juglone induces cell death of *Acanthamoeba* through increased production of reactive oxygen species. *Exp. Parasitol.* **2015**, *159*, 100−106.
(50) Anwar, A.; Shahbaz, M. S.; Saad, S. M.; Kanwal, K. M.; Khan, R.; Siddiqui, N. A.; Khan, N. A. Novel antiacanthamoebic compounds belonging to quinazolinones. *Eur. J. Med. Chem.* **2019**, *182*, 111575.

https://doi.org/10.1021/acsomega.2c06050
ACS Omega 2023, 8, 8237−8247